LA-8401-MS

The Kinematically Incomplete Breakup Reaction $^1H(\vec{d},p)pn$ at 16 MeV

University of California

LOS ALAMOS SCIENTIFIC LABORATORY
Post Office Box 1663 Los Alamos, New Mexico 87545

LA-8401-MS
UC-34c
Issued: December 1980

The Kinematically Incomplete Breakup Reaction $^{1}H(\vec{d},p)pn$ at 16 MeV

G. G. Ohlsen
F. D. Correll
Ronald E. Brown
Nelson Jarmie
R. A. Hardekopf

THE KINEMATICALLY INCOMPLETE BREAKUP REACTION

$^1H(\vec{d},p)pn$ AT 16 MeV

by

G. G. Ohlsen, F. D. Correll, Ronald E. Brown,
Nelson Jarmie, and R. A. Hardekopf

ABSTRACT

Angular distributions of the differential cross section $\sigma(E^*,\theta_1^{\ell})$ and of the vector and tensor analyzing powers $A_y(E^*,\theta_1^{\ell})$, $A_{xz}(E^*,\theta_1^{\ell})$, $A_{xx}(E^*,\theta_1^{\ell})$, and $A_{yy}(E^*,\theta_1^{\ell})$ for the 3-nucleon breakup reaction $^1H(\vec{d},p)pn$ were measured for a deuteron bombarding energy of 16.0 MeV. The data are reported as functions of the excitation energy E^* in the pn system and of the laboratory angle θ_1^{ℓ}. Laboratory angles between 15 and 42.5° were studied. The excitation energy range varies from 0-2.6 MeV at 15° to 0-0.2 MeV at 42.5°. An excitation energy range (bin) of 0.2 MeV, which corresponds to laboratory energy bins from 0.3 to 0.4 MeV, was used to partition the proton continua. The experimental laboratory energy resolution is about 0.15 MeV. Large effects are seen in the tensor analyzing powers, particularly in A_{xz}, at the lowest excitation energies. Except for A_{yy}, there is no similarity of the observed analyzing powers to the corresponding elastic-scattering analyzing powers. Some data for $A_{xz}(E^*,\theta_1^{\ell})$ at other energies are also presented.

I. INTRODUCTION

This report presents tables of the measured differential cross section $\sigma(E^*,\theta_1^{\ell})$ and tables and graphs of the measured vector and tensor analyzing powers $A_y(E^*,\theta_1^{\ell})$, $A_{xz}(E^*,\theta_1^{\ell})$, $A_{xx}(E^*,\theta_1^{\ell})$, and $A_{yy}(E^*,\theta_1^{\ell})$ for the 3-nucleon breakup reaction $^1H(\vec{d},p)pn$. The deuteron bombarding energy was 16.0 MeV for most of the measurements, but some A_{xz} data for selected angles at 12.0 to 15.0 MeV are also presented. Descriptions of the kinematics and of the experimental details are included. A preliminary version of these data was presented at the 1978 Few Nucleon Conference at Graz.[1]

II. KINEMATICS

The data in this report are presented in terms of the laboratory angle of the detected proton and in terms of 200-keV summing bins in the excitation energy of the final-state pn system. In this section we present the nonrelativistic kinematic formulas to calculate the center-of-mass angle and angular spread for each data point.

The following notation will be used. The subscripts P and T refer to the projectile and target particles, respectively. The subscripts 1, 2, and 3 refer to the three final particles. The observed final particle will be understood to be particle 1. Superscripts refer to the system of

reference with ℓ standing for the laboratory system and c for the center-of-mass system.

The energy and angle of particle 1 in the center-of-mass (c) system are related to the energy and angle in the laboratory (ℓ) system by the velocity triangle shown in Fig. 1a. V is the magnitude of the velocity of the center-of-mass system with respect to the laboratory, and is given by

$$V = (2m_p E_p^{\ell})^{1/2}/(m_p + m_T) \quad . \tag{1}$$

Because it is more convenient to work with energies, we multiply each velocity by $(\frac{1}{2} m_1)^{1/2}$ to produce an "energy triangle" as shown in Fig. 1(b), where

$$a_1 = (\tfrac{1}{2} m_1 v^2)^{1/2} = (m_1 m_p E_p^{\ell})^{1/2}/(m_p + m_T) \quad . \tag{2}$$

We may write by inspection the relations

$$E_1^{c} = E_1^{\ell} - 2a_1 (E_1^{\ell})^{1/2} \cos\theta_1^{\ell} + a_1^2 \quad , \tag{3}$$

$$\cos\theta_1^{c} = \frac{(E_1^{\ell})^{1/2} \cos\theta_1^{\ell} - a_1}{[E_1^{\ell} - 2a_1 (E_1^{\ell})^{1/2} \cos\theta_1^{\ell} + a_1^2]^{1/2}} \quad , \tag{4}$$

and

$$\phi_1^{c} = \phi_1^{\ell} \quad . \tag{5}$$

We first obtain an expression for E_1^c in terms of the excitation energy E^*. The total energy available in the center-of-mass system is

$$E_{tot} = Q + m_T E_p^{\ell}/(m_p + m_T) \quad , \tag{6}$$

where Q = -2.225 MeV. This is the total kinetic energy that is shared by the three final particles in the center-of-mass system. If particles 2 and 3, the unobserved neutron and proton, have an energy of "internal motion" of E^*, then E_a, the energy available for the motion of particle 1 and of the center of mass of the particle 2-3 system, is given by

$$E_a = E_{tot} - E^* \quad . \tag{7}$$

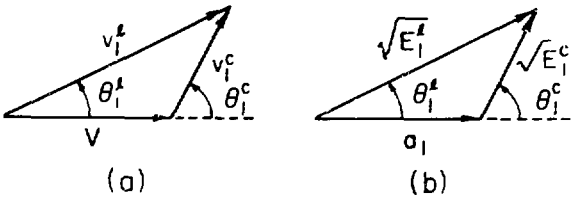

Fig. 1.
Velocity triangle and "energy triangle." V is the velocity of the center of mass and $a_1 = (\frac{1}{2} m_1 V^2)^{1/2}$.

Because particle 1 and the recoiling particle 2-3 system have equal and opposite momenta, the available energy is shared inversely as the masses of the clusters, so that the energy of particle 1 is

$$E_1^{c} = \frac{m_2 + m_3}{m_1 + m_2 + m_3} [E_{tot} - E^*] \quad . \tag{8}$$

When we combine Eqs. (6) and (8) and specialize to the present H(d,p)pn case using integer masses, we find

$$E_1^{c} = \frac{2}{3} [-2.225 - E^* + \frac{1}{3} E_p^{\ell}] \quad . \tag{9}$$

where, in Eq. (9) and those that follow, the energies are expressed in MeV.

Equation (3) may be solved for $(E_1^{\ell})^{1/2}$:

$$(E_1^{\ell})^{1/2} = a_1 \cos\theta_1^{\ell} \pm [(a_1 \cos\theta_1^{\ell})^2 - a_1^2 + E_1^{c}]^{1/2} \quad . \tag{10}$$

With the present values of the masses, a_1 becomes equal to $(2E_p/9)^{1/2}$, and Eq. (10) becomes

$$(E_1^{\ell})^{1/2} = \left(\frac{2E_p^{\ell}}{9}\right)^{1/2} \gamma \quad , \tag{11}$$

with

$$\gamma = \cos\theta_1^{\ell} \pm \left(\cos^2\theta_1^{\ell} - \frac{3}{E_p^{\ell}} (2.225 + E^*)\right)^{1/2} \quad . \tag{12}$$

Substitution of this result into Eq. (4) gives the desired expression for θ_1^c in terms of E^* and θ_1^ℓ:

$$\cos\theta_1^c = \frac{\gamma\cos\theta_1^\ell - 1}{(\gamma^2 - 2\gamma\cos\theta_1^\ell + 1)^{1/2}} \quad . \tag{13}$$

In Fig. 2, the center-of-mass angle θ_1^c is plotted vs E^* for various values of θ_1^ℓ. Note that θ_1^c is explicitly a function of E^*, so that there is no uniquely defined value of θ_1^c for an energy bin of finite width in E^*. Thus, the primary presentation of our data is as a function of E^* and θ_1^ℓ. In the reaction ^{1}H(d⃗,p)pn the target is lighter than the projectile, and therefore we obtain double-valued kinematic functions [± in Eq. (12)]. Here our interest is confined to the higher lab-energy branch of any such functions. The above kinematic discussion is adapted from Ref. 2, which should be consulted for additional details.

III. EXPERIMENT

A. Apparatus and Procedure

The experiment was performed at the Los Alamos Scientific Laboratory (LASL) Van de Graaff facility[3] using the FN tandem Van de Graaff accelerator and the Lamb-shift polarized ion source.[4,5] The scattering chamber used is a 61-cm cube[6,7] called the "supercube." Among its many features[6,7] are four independently rotatable turntables for mounting detectors in each of four azimuthal quadrants and the capability of being rotated about the beam direction. We used only two of the turntables, but did rotate the supercube as part of the data-taking procedure.

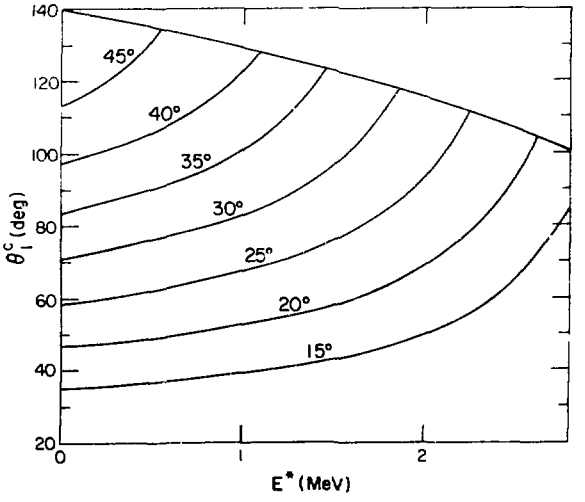

Fig. 2.
The center-of-mass angle θ_1^c vs the pn energy E^* for several values of the laboratory angle θ_1^ℓ for the reaction ^{1}H(d,p)pn at 16 MeV. The proton lab energy E_1^ℓ is a double-valued function of E^*; the curves apply to the branch corresponding to the larger values of E_1^ℓ. The top curve is a limiting curve for this upper branch of the E_1^ℓ vs E^* function.

A 9.7-cm-diam gas target cell was used for the measurements. This target cell has a beam-entrance snout about 6 cm long. A 2.5-μm-thick Havar* foil covered the 2.5-mm-diam beam-entrance aperture on the snout, and a 7-μm-thick Kapton** foil covered the 300° cell opening through which the beam and detected particles emerged. The target was operated at a pressure near 300 Torr and at room temperature. Temperature and pressure were monitored. The target gas was flushed occasionally.

A polarized deuteron beam of 8 to 120 nA was used during the experiment. At the most forward angles, the beam current had to be limited to keep the counting losses at an acceptable level, generally below 10%. These losses, coming mainly from the analog-to-digital converters, were measured and used to correct the data.

The spin-quantization axis was always positioned in the horizontal plane, and the angle β between this axis and the beam direction was set to an accuracy[8] of about ±0.5°. The beam was aligned and its position monitored by means of two sets of four-way slits, one set at the entrance to the supercube and the other in the Faraday cup assembly.

Our measurement technique was very similar to the "three spin state method" discussed in Ref. 9. The only difference was that the use of two turntables instead of four required us to rotate the supercube through 90° to obtain data at the necessary four azimuthal angles. Thus, data for each of the three spin states m_1 were obtained in each of the following three configurations.

(1) β = 90°, detectors in the horizontal plane, to determine A_{xx}.

(2) β = 90°, detectors in the vertical plane, to determine A_y and A_{yy}.

(3) β = 45°, detectors in the horizontal plane, to determine A_{xz}. (A_{yy} can also be extracted, but less accurately than in the second configuration.)

This data-taking technique is illustrated in Fig. 3.

*Havar is the trade name for a cobalt "superalloy" manufactured by Hamilton Technology, Inc., Lancaster, PA 17604.
**Kapton is a polyimide film made by E. I. Du Pont de Nemours and Company, Wilmington, DE 19898.

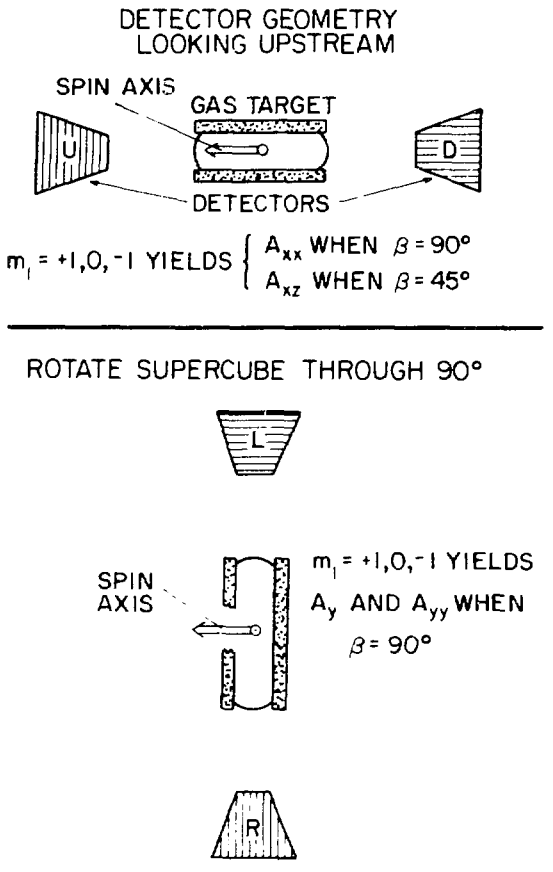

Fig. 3.
Use of the "three spin state method" (Ref. 9) for measuring analyzing powers with a polarized deuteron beam.

The relative polarizations p_z and p_{zz} (neglecting the unpolarized background) in the spin states used are given by[6,8]

$$m_I = 1: p_z = 1,\ p_{zz} = 1,$$
$$"m_I = 0": p_z = 0.012,\ p_{zz} = -1.965,$$

and

$$"m_I = -1": p_z = -0.984,\ p_{zz} = 0.952.$$

Those states labeled with quotation marks contain small admixtures of states with other m_I values. The absolute beam polarizations are obtained by multiplying p_z and p_{zz} by p_Q, the fraction of the total beam that is actually polarized. This fraction was determined by the quench-ratio technique[10,11] and typically had values near 0.82. This method results in the beam polarizations being known to about ±1.5%.

On-line data processing, control of some of the supercube and ion-source functions, and capacitance-manometer monitoring of the gas-target pressure were carried out with the LASL Van de Graaff MODCOMP IV/25 computer system.

Each of the two detector assemblies consisted of an 86.5-μm ΔE silicon detector and a 1500-μm E silicon surface barrier detector mounted behind a standard gas-target collimator arrangement, which had an angular acceptance of 1/2° (full width at half maximum). The detectors were cooled with thermo-electric devices. A separate analog-to-digital converter was used for each detector, and protons were identified by appropriate processing of these digitized signals by the on-line computer.

The experimental energy resolution, inferred from the width of the group arising from elastic scattering in the process $^1H(d,p)^2H$, was found to be about 130 keV for one detector stack (No. 0) and 150 keV for the other detector stack (No. 2). The data are presented in terms of increments in excitation energy E^* of the residual pn system. From kinematics it can be deduced that $\Delta E^*/\Delta E_1^{\ell}$ ranges from 1.6 to 2.0, so in terms of E^*, the effective energy resolution is 70 or 80 keV, which is substantially smaller than the 200-keV step in E^* chosen for our data presentation. A typical pulse height spectrum is presented in Fig. 4.

B. Errors

The elastic analyzing powers have relative errors that are a quadratic combination of the error due to counting statistics and an additional relative error of 0.005.[8] This additional error is based on the data repeatability experienced over the years for this type of experiment and arises from such effects as fluctuations in the p_Q measurement, fluctuations in beam position, and uncertainties in background subtraction and beam-current integration. There is also a scale error of 1.5% from the determination of the absolute beam polarization.

The measurement of analyzing powers in a continuum is subject to an error from "binning" that is not present when well-resolved discrete groups are measured. This results from drifts in the energy calibration and/or resolution functions of the two detectors, and, to some extent, from "quantization errors" associated with selection of a discrete number of channels for summing.

In the present case, separate energy calibrations for each detector stack were carried out by means of $^1H(d,p)$

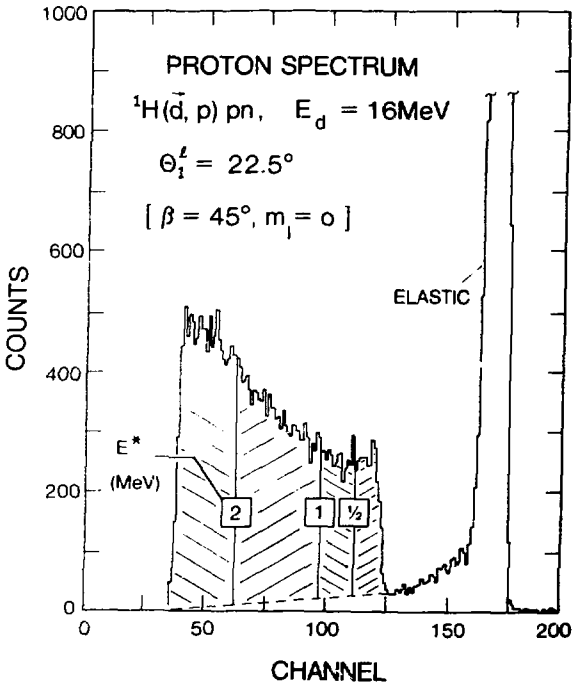

Fig. 4.
A proton spectrum at E_d = 16 MeV, θ_1^ℓ = 22.5 ° for the m_1 = 0 state. Excitations of E* = 0.5, 0.1, and 2.0 MeV are indicated.

elastic scattering. The calibration was in terms of the calculated proton energy at the center of the target. In this way, the calibration constants directly determine the energy of interest, and no account has to be taken of the energy loss of the reaction protons as they traverse the gas target and exit foil.

A pulse height resolution of 512 channels was used. The energy calibration data were fitted with a quadratic curve of the form $E = a_0 + a_1c + a_2c^2$, where E is the proton energy (at target center) in MeV and c is the channel number. The constants obtained were:

Detector No.	a_0	a_1	a_2
0	-0.16427	0.28316 × 10 ⁻¹	0.31089 × 10 ⁻⁵
2	-0.06381	0.27858 × 10 ⁻¹	0.36989 × 10 ⁻⁵

These results reflect only minor deviations from linearity.

A computer code was used to calculate and set the channels that were used to divide the continuum proton spectra into equal steps in E*. The data were processed using both a 0.1-MeV and a 0.2-MeV step in E*. A comparison of the results for the 0.1-MeV step size with those for the 0.2-MeV step size is shown in Fig. 5 for $A_{xz}(E^*, \theta_1^\ell = 27.5°)$. Considering the statistics, the energy

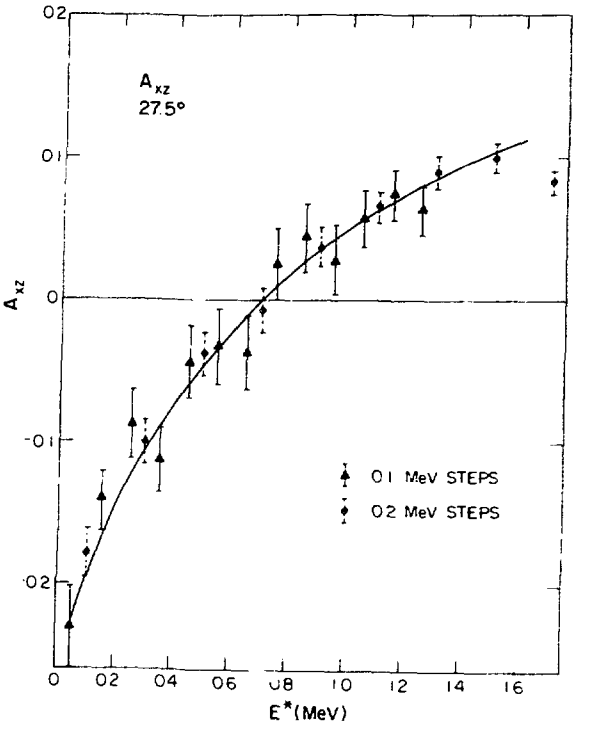

Fig. 5.
The observed analyzing power A_{xz} at θ_1^ℓ = 27.5° vs excitation energy E* for 0.1- and 0.2 MeV intervals in E* The curve is to guide the eye.

dependence is well represented by using a 0.2-MeV step size. Thus, we conclude that no information is lost by reporting the data in 0.2-MeV steps, so this step size is adopted in this report.

For 0.2-MeV steps, the summing interval was typically 9 or 10 channels. Thus, a rounding difference of one channel between the spectra recorded in the two detector stacks could result in a yield difference of about 10% in the corresponding summing bins. This does not seriously affect the analyzing powers, however, as our method extracts an observed quantity from each detector stack (three spin sequences) separately, and only then are the two results combined. If the electronics and accelerator were perfectly stable, the binning problem would affect only the energy resolution of the measured quantities. However, drifts during a three spin counting sequence could introduce genuine errors. These effects can best be estimated from the consistency of the data, which appears to be better than ±0.02 for each of the analyzing-power observables.

Although the experiment and data analysis were not originally set up to recover cross-section information, reasonably good values can be extracted. For the elastic scattering cross sections, relative values are accurate to within ±2%, with an absolute normalization uncertainty of ±5%.

For the breakup cross sections, the previously mentioned binning error can cause errors of up to 10% for cross sections. Values were obtained by averaging the yield results from the A_{xz}, $A_y + A_{yy}$, and A_{xx} measurement sets, so this is expected to mitigate the binning error somewhat. Nevertheless, we assigned a relative accuracy of ±10% to the cross-section determinations, together with an absolute normalization uncertainty of ±5%.

IV. RESULTS AND DISCUSSION

Complete angular distributions of $A_y(E^*,\theta_1^Q)$, $A_{yy}(E^*,\theta_1^Q)$, $A_{xx}(E^*,\theta_1^Q)$, $A_{yy}(E^*,\theta_1^Q)$, and the differential cross section $\sigma(E^*,\theta_1^Q)$ for the reaction $^1H(\vec{d},p)pn$ were obtained at E_d = 16.0 MeV. These results, along with the results simultaneously obtained for the elastic-scattering process, are presented in Tables I-V. Additional data at a few angles and at 12.0, 13.0, 14.0, and 15.0 MeV are summarized in Table VI.

The 16-MeV elastic-scattering analyzing power angular distributions are compared in Fig. 6 with the E^* = 0-0.2 MeV excitation-energy results. These data are plotted vs the center-of-mass angle of the observed protons. As previously noted, in the inelastic case there is a kinematic spread in the center-or-mass angle for a finite E^* step. This spread varies from about 1 to 4° over the angular range of Fig. 6. For A_{xx} and A_{xz}, large differences between the elastic and inelastic values are observed. Although this is not a particularly surprising result, because the elastic scattering leads to a triplet final pn state whereas inelastic scattering at energies near the breakup threshold leads to a mixture of singlet and triplet final pn states, it is in contradiction to some earlier $\vec{p}$+d results at 22.7-MeV proton energy[12] and $\vec{d}$ + d results at 21-MeV deuteron energy.[13] These earlier results showed that, for the E^* interval of 0-1 MeV, the inelastic vector analyzing powers were smaller in magnitude, but similar in angular shape, to the corresponding elastic vector analyzing power. Based on the differential cross-section results of Brückman et al.[14], who deduced that, at least at some angles, the cross section is dominated by the singlet final-state contribution. Rad et al.[12] concluded that triplet contributions were unexpectedly more important than Brückman's result would lead one to expect. From the present experiment, however,

TABLE I

ANALYZING POWER A_y FOR $^1H(\vec{d},p)pn$ AT LAB ENERGY 16 MeV

Range in E^* (MeV)	15°	17.5°	20°	25°	30°	35°	40°	42.5°
Elastic	0.0298(09)[a]	0.0385(10)	0.0528(11)	0.0701(16)	0.0679(20)	0.0367(20)	0.0183(11)	0.0120(15)
0.0 0.2	0.0145(95)	0.001 (11)	0.024 (11)	0.003 (14)	0.000 (15)	0.024 (16)	0.0115(95)	0.017 (14)
0.2 0.4	0.0147(79)	-0.0109(84)	0.0303(91)	0.007 (12)	0.031 (13)	0.028 (13)	0.0041(72)	
0.4 0.6	0.0152(77)	0.0099(85)	0.0219(88)	0.014 (12)	0.005 (12)	0.009 (12)	0.0010(62)	
0.6 0.8	0.0155(74)	0.0062(82)	0.0020(88)	0.001 (11)	0.019 (12)	0.006 (11)		
0.8 1.0	0.0010(73)	0.0009(78)	0.0173(83)	0.018 (10)	0.005 (10)	0.0068(89)		
1.0 1.2	0.0121(70)	0.0087(74)	0.0075(79)	0.0152(92)	0.0117(87)	0.0056(72)		
1.2 1.4	0.0013(67)	0.0054(71)	0.0170(72)	0.0035(86)	0.0050(75)			
1.4 1.6	0.0045(66)	0.0090(68)	0.0126(69)	0.0007(72)	0.0261(62)			
1.6 1.8	0.0059(63)	0.0012(64)	0.0018(62)	0.0129(65)				
1.8 2.0	0.0014(60)	0.0022(60)	0.0032(58)	0.0140(52)				
2.0 2.2	0.0033(58)	0.0067(55)	0.0098(50)					
2.2 2.4	0.0028(54)	0.0026(47)	0.0055(39)					
2.4 2.6	0.0070(47)	0.0066(36)						

[a]The numbers in parentheses give the error resulting from counting statistics and refer to the two least significant digits. The relative errors are larger than this. For the elastic data the relative errors are quadratic combination of the error due to counting statistics and an additional error of 0.005. For the breakup data the relative errors are 0.02. There is also a scale error in all the data of 1.5%.

TABLE II

ANALYZING POWER A_{y} FOR $^{1}H(\vec{d},p)pn$ AT LAB ENERGY 16 MeV

Range in E* (MeV)	15°	17.5°	20°	22.5°	25°	27.5°	30°	32.5°	35°	37.5°	40°	42.5°
Elastic	0.0216(23)[a]	0.0021(16)	0.0208(15)	0.0521(18)	0.0774(22)	0.0833(25)		0.0238(28)	0.0138(28)	0.0490(24)	0.0633(23)	0.0732(23)
0.0 0.2	0.065 (22)	0.061 (16)	0.091 (14)	0.165 (16)	0.185 (19)	0.177 (17)	0.205 (20)	0.216 (17)	0.223 (20)	0.187 (18)		0.124 (17)
0.2 0.4	0. 02 (19)	0.040 (14)	0.037 (13)	0.059 (15)	0.104 (17)	0.099 (16)	0.141 (18)	0.130 (16)	0.149 (18)	0.120 (16)		
0.4 0.6	0.016 (19)	0.017 (14)	0.017 (13)	0.052 (15)	0.018 (16)	0.037 (16)	0.052 (17)	0.056 (15)	0.061 (17)	0.058 (14)		
0.6 0.8	0.031 (18)	0.024 (14)	0.030 (12)	0.005 (14)	0.030 (16)	0.008 (16)	0.003 (16)	0.006 (14)	0.005 (15)	0.006 (12)		
0.8 1.0	0.093 (18)	0.041 (13)	0.075 (12)		0.061 (15)	0.036 (14)	0.021 (14)	0.039 (12)	0.016 (13)			
1.0 1.2	0.079 (18)	0.054 (13)	0.086 (11)		0.087 (13)	0.066 (13)	0.053 (12)	0.033 (11)	0.0219(99)			
1.2 1.4	0.062 (16)	0.101 (12)	0.105 (10)	0.112 (11)	0.084 (12)	0.091 (11)	0.069 (11)	0.0606(89)				
1.4 1.6	0.096 (16)	0.111 (11)	0.1193(95)	0.109 (10)	0.099 (11)	0.0998(98)	0.0728(86)					
1.6 1.8	0.075 (16)	0.102 (11)	0.1251(89)	0.1015(90)	0.1231(89)	0.0831(80)						
1.8 2.0	0.104 (15)	0.117 (10)	0.1192(78)	0.0963(80)	0.0874(73)							
2.0 2.2	0.085 (14)	0.1071(92)	0.1202(68)	0.1017(63)								
2.2 2.4	0.095 (14)	0.1066(80)	0.1047(55)									
2.4 2.6	0.099 (12)	0.0945(60)										

[a]See the footnote to Table I.

TABLE III

ANALYZING POWER A_{xx} FOR $^{1}H(\vec{d},p)pn$ AT LAB ENERGY 16 MeV

Range in E* (MeV)	15°	17.5°	20°	22.5°	25°	27.5°	30°	32.5°	35°	37.5°	40°	42.5°
Elastic	-0.0927(12)[a]	0.1150(15)	0.1417(19)	0.1473(23)	0.1501(28)	0.1259(31)	0.0906(35)	0.0555(27)	0.0351(27)	0.0238(37)	0.0312(36)	0.0411(25)
0.0 0.2	-0.022 (12)	0.010 (15)	0.006 (18)	0.033 (20)	0.063 (23)	0.047 (22)	0.015 (24)	0.027 (19)	0.081 (21)	0.111 (33)	0.098 (34)	-0.145 (24)
0.2 0.4	0.020 (11)	0.025 (13)	0.023 (16)	0.001 (18)	0.031 (21)	0.050 (20)	0.048 (22)	0.038 (17)	0.069 (18)	0.066 (25)	-0.084 (25)	
0.4 0.6	-0.022 (10)	0.008 (13)	0.053 (16)	0.004 (18)	0.028 (20)	0.026 (20)	0.055 (21)	0.024 (16)	0.051 (16)	0.056 (23)	0.107 (21)	
0.6 0.8	0.052 (10)	0.065 (13)	0.034 (15)	0.046 (18)	0.036 (20)	0.001 (20)	0.021 (19)	0.035 (15)	0.027 (14)	0.067 (19)		
0.8 1.0	-0.0383(98)	0.033 (12)	0.042 (15)	0.047 (17)	0.037 (18)	0.004 (17)	0.029 (17)	0.037 (13)	0.024 (12)			
1.0 1.2	-0.0511(95)	0.053 (12)	0.054 (14)	0.042 (15)	0.004 (16)	0.014 (16)	0.057 (15)	0.026 (11)	0.0302(98)			
1.2 1.4	0.0438(90)	0.055 (11)	0.045 (13)	0.008 (14)	0.010 (15)	0.010 (14)	0.012 (13)	0.0232(89)				
1.4 1.6	0.0379(89)	0.049 (11)	0.047 (13)	0.030 (13)	0.004 (12)	0.039 (12)	0.017 (1[illegible]					
1.6 1.8	-0.0505(84)	0.0350(99)	0.013 (11)	0.015 (11)	0.008 (11)	0.0147(97)						
1.8 2.0	0.0285(81)	0.0449(94)	0.0331(99)	0.004 (10)	0.0067(87)							
2.0 2.2	-0.0353(78)	0.0385(86)	0.0333(86)	0.0250(79)								
2.2 2.4	0.0373(73)	0.0242(73)	0.0050(67)									
2.4 2.6	0.0335(63)	0.0248(56)										

[a]See the footnote to Table I.

TABLE IV

ANALYZING POWER A_{yy} FOR $^1H(\vec{d},p)pn$ AT LAB ENERGY 16 MeV

Range in E* (MeV)	15°	17.5°	20°	25°	30°	35°	40°	42.5°
Elastic	0.0247(16)[a]	0.0380(16)	0.0612(18)	0.1109(26)	0.1514(33)	0.1397(33)	0.1149(18)	0.0984(24)
0.0-0.2	0.055 (16)	0.074 (18)	0.109 (19)	0.107 (23)	0.138 (24)	0.130 (26)	0.118 (16)	0.170 (23)
0.2-0.4	0.047 (14)	0.048 (14)	0.095 (15)	0.083 (20)	0.078 (22)	0.104 (22)	0.083 (12)	
0.4-0.6	0.039 (13)	0.057 (15)	0.037 (15)	0.076 (19)	0.045 (21)	0.079 (21)	0.081 (10)	
0.6-0.8	0.012 (13)	0.016 (14)	0.027 (15)	0.085 (19)	0.074 (20)	0.080 (18)		
0.8-1.0	0.020 (13)	0.032 (13)	0.019 (14)	0.073 (17)	0.045 (17)	0.045 (15)		
1.0-1.2	0.005 (12)	0.024 (13)	0.028 (14)	0.044 (16)	0.052 (15)	0.037 (12)		
1.2-1.4	0.012 (12)	0.020 (12)	0.026 (12)	0.040 (15)	0.062 (13)			
1.4-1.6	−0.004 (12)	−0.018 (12)	0.035 (12)	0.012 (12)	0.050 (11)			
1.6-1.8	−0.013 (11)	0.003 (11)	0.029 (11)	0.023 (11)				
1.8-2.0	0.011 (11)	0.004 (11)	0.0255(99)	0.0326(88)				
2.0-2.2	−0.006 (10)	0.0098(96)	0.0251(85)					
2.2-2.4	0.0028(94)	0.0165(82)	0.0189(67)					
2.4-2.6	0.0174(81)	0.0081(62)						

[a]See the footnote to Table I.

TABLE V

DIFFERENTIAL CROSS SECTION (mb/sr-MeV) FOR $^1H(d,p)pn$ AT 16 MeV

Range in E* (MeV)	15°	17.5°	20°	22.5°	25°	27.5°	30°	32.5°	35°	37.5°	40°	42.5°
Elastic (mb/sr)	371.6[a]	292.9	211.0	158.0	121.9	100.5	90.6	90.3	96.0	105.8	118.8	133.1
0.0-0.2	26.0[b]	19.1	15.5	13.6	11.6	13.1	11.3	11.0	11.2	11.1	9.9	10.1
0.2-0.4	31.6	24.0	18.3	15.0	13.1	14.3	12.7	12.4	13.7	13.8	14.7	
0.4-0.6	32.7	23.6	18.5	13.7	13.7	13.9	14.4	14.1	15.1	16.8	19.3	
0.6-0.8	34.7	25.1	19.1	16.0	14.1	14.5	15.9	16.5	20.0	22.6		
0.8-1.0	35.4	27.0	20.7	17.8	16.6	17.6	19.8	22.4	25.6			
1.0-1.2	37.3	28.5	22.6	20.3	20.0	20.0	26.4	28.9	39.7			
1.2-1.4	41.3	31.0	26.4	23.5	22.8	26.5	33.8	42.7				
1.4-1.6	41.5	33.5	28.7	27.6	30.3	34.7	50.2					
1.6-1.8	45.5	37.8	34.0	34.9	38.3	51.9						
1.8-2.0	49.5	41.5	40.4	43.6	58.4							

[a]The elastic data have relative errors of 2% and a scale error of 5%.
[b]The breakup data have relative errors of 10% and a scale error of 5%.

one sees that E* = 0-1 MeV is far too large an interval to allow clear information about the effect of the singlet state to be extracted.

Except for a recent measurement of the proton observable A_y at 21 MeV and $\theta_l = 75°$,[15] the present data are the first analyzing-power data reported with energy resolution better than 0.5 or 1 MeV. Overall views of the angular distributions of each analyzing power for the various E* bins are given in Figs. 7-10.

Earlier data obtained at LASL on this process were presented at the 1978 Few Nucleon Conference in Graz.[1] The present data are of higher quality, and in particular have better energy resolution. The A_{xz} effect, which shows the largest deviation from the elastic-scattering results, approximately doubles when the summing bin size is reduced from 0.5 MeV (Graz) to 0.2 MeV (present analysis). Data obtained with an even finer intrinsic resolution in E* than the 70 or 80 keV employed in this experiment might reveal additional information, but from the comparison of 0.1- and 0.2-MeV intervals in Fig. 5 it appears unlikely.

TABLE VI

A_{xz} EXCITATION FUNCTIONS

Range in E^* (MeV)	E_d 16 (MeV) θ_l^c = 40°	15 40°	16 32.5°	15 32.5°	14 32.5°	13 32.5°	12 32.5°	16 22.5°	14 22.5°	12 22.5°
Elastic	0.0633(23)[a]	0.0544(19)	0.0238(28)	0.0350(23)	0.0397(19)	0.0416(18)	0.0459(17)	0.05[illegible]1(18)	0.0425(19)	0.0327(16)
0.0 0.2		0.156 (17)	0.216 (17)	-0.226 (17)	-0.198 (14)	-0.182 (14)	-0.154 (13)	0.165 (16)	0.144 (18)	0.139 (18)
0.2 0.4		0.095 (12)	0.130 (16)	-0.134 (15)	-0.101 (12)	-0.099 (11)		0.059 (15)	0.042 (16)	0.026 (16)
0.4 0.6			0.056 (15)	-0.033 (14)	-0.038 (11)	-0.0182(92)		0.052 (15)	0.013 (17)	0.004 (15)
0.6 0.8			0.006 (14)	0.008 (12)	-0.0041(89)			0.005 (14)	0.069 (15)	0.032 (13)
0.8 1.0			0.039 (12)	0.012 (10)					0.072 (14)	0.0634(99)
1.0 1.2			0.033 (11)							
1.2 1.4			0.0?06(89)					0.112 (11)		
1.4 1.6								0.109 (10)	0.0976(83)	
1.6 1.8								0.1015(90)		
1.8 2.0								0.0963(80)		

[a] See the footnote to Table I.

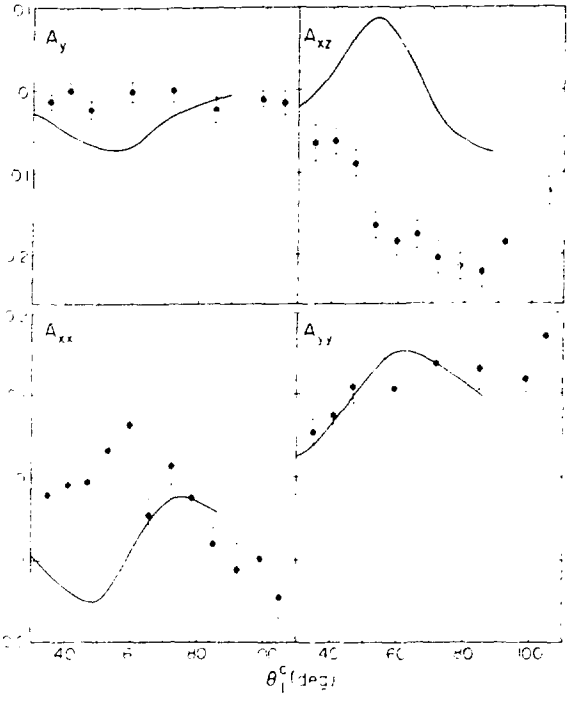

Fig. 6.
Observed analyzing powers for the elastic-scattering process $^1H(\vec{d},p)^2H$ (*solid line*) and for the breakup reaction $^1H(\vec{d},p)pn$ with $E^* = 0$-0.2 MeV (points) vs the center-of-mass angle θ_l^c.

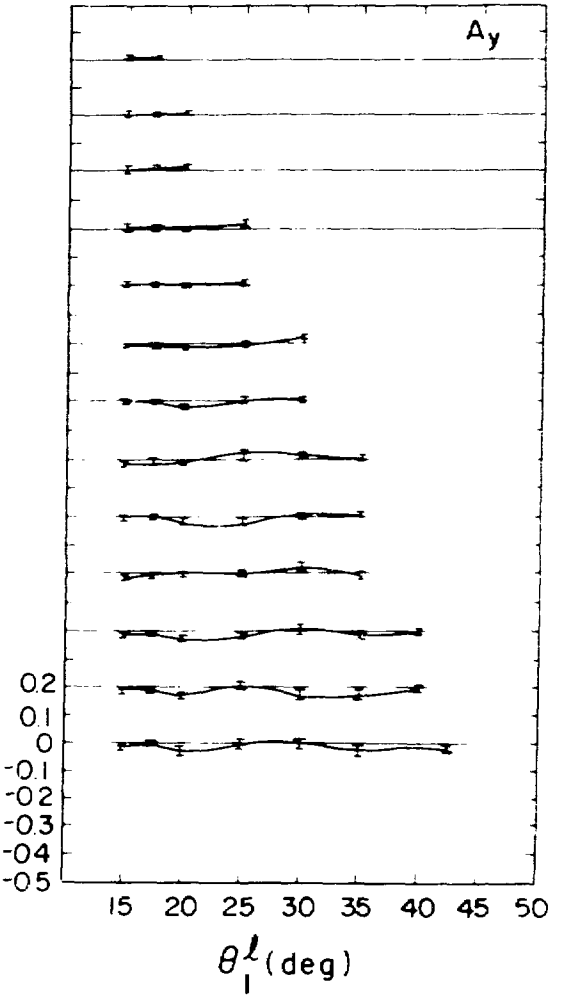

Fig. 7.
Graph of $A_y(\theta_l^l, E^*)$. The numbers for the vertical scale refer to the bottom graph, which is for the excitation interval 0 to 200 keV. Successively higher graphs are for successively higher 200-keV excitation intervals, and are displaced successively upwards by 0.2 in analyzing power.

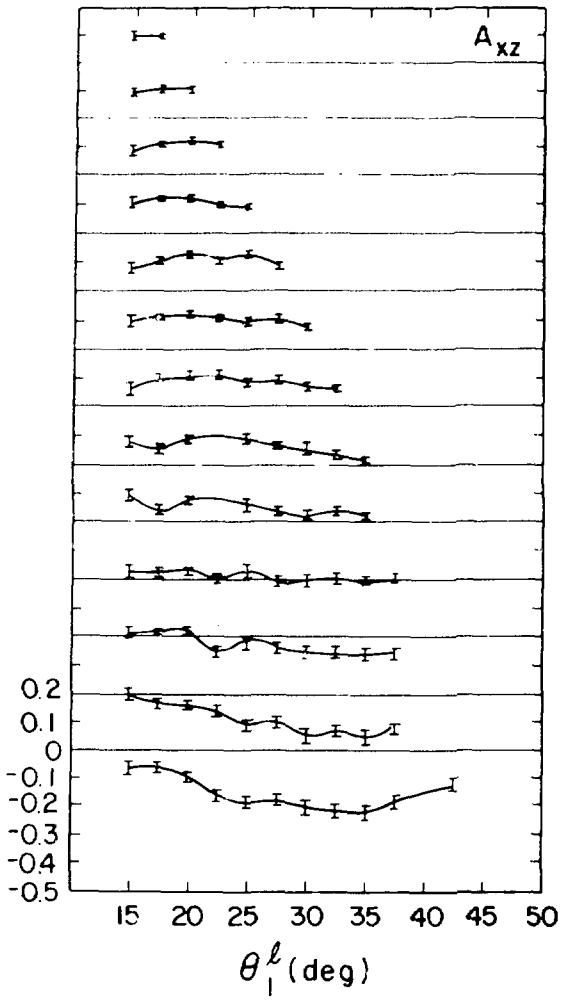

Fig. 8.
Graph of $A_{xz}(\theta_1^{\ell},E^*)$; see the caption to Fig. 7.

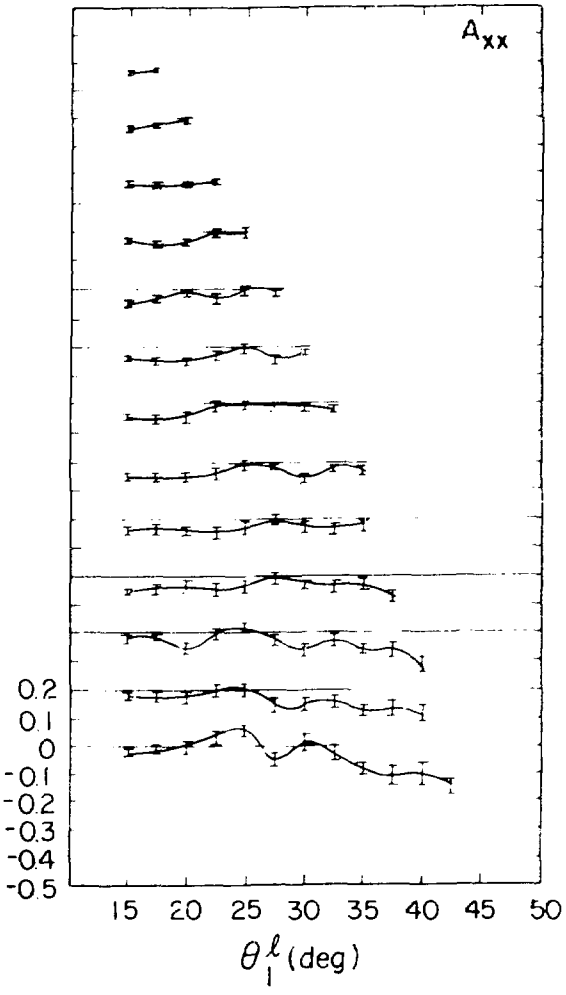

Fig. 9.
Graph of $A_{xx}(\theta_1^{\ell},E^*)$; see the caption to Fig. 7.

Faddeev calculations of $A_y(E^*,\theta_1^{\ell})$ for 22.7-MeV protons,[16,17] which assumed $E^* = 0$, disagreed with the experimental observations. As mentioned, however, these observations were averaged over a 1-MeV interval, whereas we are dealing with a structure not wider than a few hundred keV (Fig. 5). Therefore, it would be of great interest if some $E^* = 0$ calculations for the present observables and bombarding energy were to become available.

A view of the data in broad perspective appears to reveal two main features.

(1) The energy width of the effect at low excitation energy, presumably caused by the singlet final-state interaction, is several hundred keV. It is most clearly observed in A_{xz}, although A_{xx} indicates a similar width. The clarity of this effect of the singlet state could lead to new insights as to its properties.

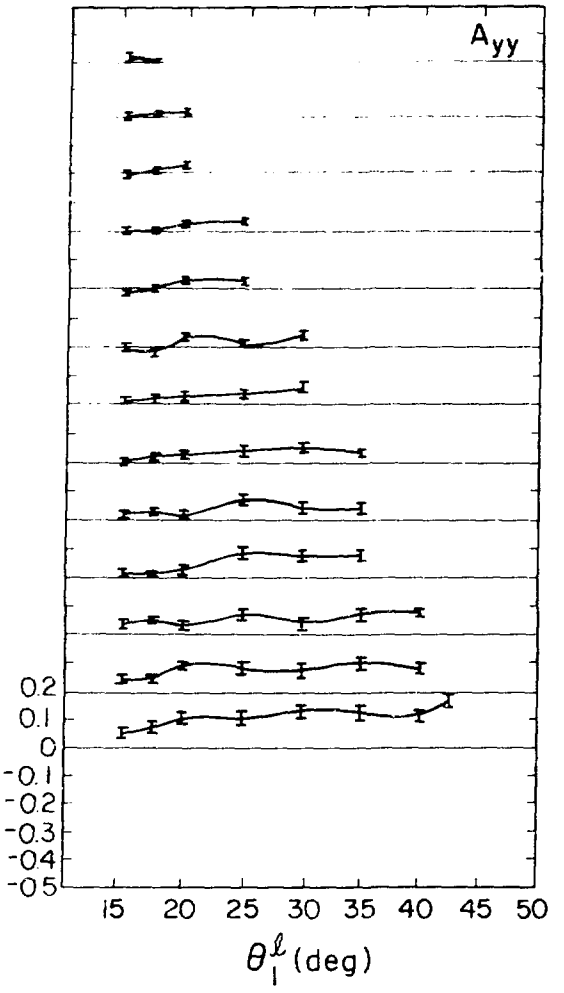

Fig. 10.

Graph of $A_{yy}(\theta_1^{\ell},E^*)$; see the caption to Fig. 7.

(2) At the higher excitation energies, the analyzing powers tend to reach an asymptotic value that is more or less independent of angle

$A_y \sim 0.00 \pm 0.02$,

$A_{xz} \sim 0.10 \pm 0.02$,

$A_{xx} \sim -0.02 \pm 0.02$,

and

$A_{yy} \sim 0.02 \pm 0.02$.

Once again, A_{xz} seems to exhibit the strongest effect. There may be a simple geometrical interpretation of these facts along the lines of the classical 3-body breakup of an object with angular momentum, but the authors have not yet formulated such a picture.

The $A_{xz}(E^*,\theta_1^{\ell})$ excitation functions obtained at $\theta_1^{\ell} = 22.5°$ and at $\theta_1^{\ell} = 32.5°$ for $E^* = 0$-0.2 MeV are presented in Fig. 11. A slight increase in absolute magnitude with increasing energy is evident.

V. CONCLUSION

We have observed large effects in the A_{xz} and A_{xx} analyzing powers for the reaction $^1H(\vec{d},p)pn$, and have shown that a resolution of 200 keV or better is necessary to reveal the structure of the reaction, which appears to have a width of only several hundred keV in E^*. For the 0- to 200-keV range in E^*, Faddeev calculations for $E^* = 0$ may have some relevance, although calculations averaged over the kinematic configurations actually included in the 0- to 200-keV range would be preferable.

Large differences between the elastic and the $E^* = 0$- to 0.2- MeV inelastic analyzing powers have been observed.

V. ACKNOWLEDGMENT

The authors wish to thank J. L. McKibben of LASL Group P-9 for his help with the polarized ion source.

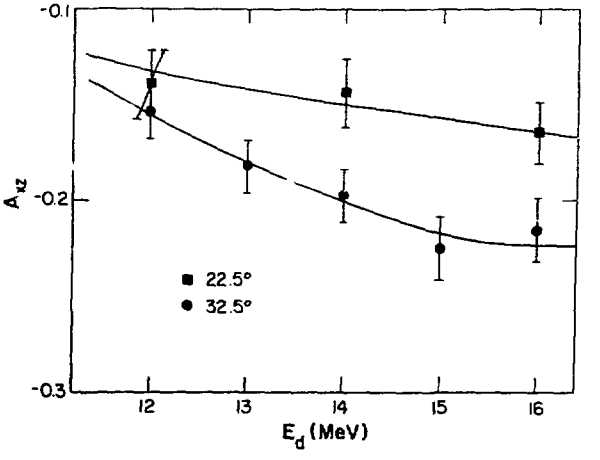

Fig. 11.

A_{xz} vs deuteron bombarding energy for the reaction $^1H(\vec{d},p)pn$ at $\theta_1^{\ell} = 22.5°$ and $\theta_1^{\ell} = 32.5°$ The excitation energy interval is 0-0.2 MeV. The curves are to guide the eye.

REFERENCES

1. G. G. Ohlsen, "Polarization Effects in the 3-body Syste :," in *Few Body Systems and Nuclear Forces, II*, H. Zingl, M. Haftel, and H. Zankel, Eds., Lecture Notes in Physics 87 (Springer-Verlag, 1978), p. 295.

2. G. G. Ohlsen, "Kinematic Relations in Reactions of the Form A + B → C + D + E," Nucl. Instrum. Methods 37, 240 (1965).

3. *R. Woods, J. L. McKibben, and R. L. Henkel,* "The Los Alamos Three-Stage Van de Graaff Facility," Nucl. Instrum. Methods **122**, 81 (1974).

4. G. P. Lawrence, G. G. Ohlsen, and J. L. McKibben, "Source of Polarized Negative Hydrogen and Deuterium Ions," Phys. Lett. **28B**, 594 (1969).

5. J. L. McKibben, G. P. Lawrence, and G. G. Ohlsen, "Performance of the LASL Polarized Source," in *Polarization Phenomena in Nuclear Reactions*, H. H. Barschall and W. Haeberli, Eds., Proc. 3rd Int. Symp., Madison, 1970 (University of Wisconsin, Madison, Wisconsin, 1971), p. 828.

6. P. A. Lovoi, "Proton-Proton Analyzing Power Measurements at 16 MeV," Los Alamos Scientific Laboratory report *LA-6041-T (September 1975).*

7. G. G. Ohlsen and P. A Lovoi, "The 'Supercube' Scattering Chamber for Spin-1/2 and Spin-1 Analyzing Power Measurements," in *Proc. 4th Int. Symp. on Polarization Phenomena in Nuclear Reactions*, Zürich, 1975, W. Grüebler and V. König, Eds. (Birkhäuser, Basel, 1976), p. 907.

8. G. G. Ohlsen, P. A. Lovoi, G. C. Salzman, U. Meyer-Berkhout, C. K. Mitchell, and W. Grüebler, "Analyzing Power for d - ^{4}He Elastic Scattering at 12.0, 14.0, and 17.0 MeV," Phys. Rev. *C* **8**, *1262* (1973).

9. G. G. Ohlsen and P. W. Keaton, Jr., "Techniques for Measurements of Spin-1/2 and Spin-1 Polarization Analyzing Tensors," Nucl. Instrum. Methods **109**, 41 (1973).

10. G. G. Ohlsen, G. P. Lawrence, P. W. Keaton, Jr., J. L. McKibben and D. D. Armstrong, "Absolute Beam Polarization Determination for the LASL *Lamb-Shift* Source by the Quench Ratio Method," in *Polarization Phenomena in Nuclear Reactions*, H. H. Barschall and W. Haeberli, Eds., Proc. 3rd Int. Symp., Madison, 1970 (University of Wisconsin, Madison, Wisconsin, 1971), p. 842.

11. G. G. Ohlsen, J. L. McKibben, G. P. Lawrence, P. W. Keaton, Jr., and D. D. Armstrong, "Precise Proton-Polarization Standard Determined with a Lamb-Shift Ion Source Incorporating a Spin Filter," *Phys. Rev. Lett. 27*, 599 (1971)

12. F. N. Rad, H. E. Conzett, R. Roy, and F. Seiler, "Polarization Effects in the Final-State Interaction Region of the p - d Breakup Reaction," Phys. Rev. *Lett. 35* 1134(1975).

13. J. Sanada, S. Seki, T. Tagishi, Y. Takeuchi, M. Sawada, and K. Furono, "Elastic and Inelastic D + d Scattering at 21 MeV," in *Proceeding of the International Conference on Nuclear Structure*, Tokyo, 1977, T. Marumori, Ed., J. Phys. Soc. Jpn. **44**, Suppl. 577 (1978), p.8.

14. H. Brückman, W. Kluge, H. Matthäy, L. Schänzler, and K. Wick, "The Angular Distribution of Final-State Interacting n - p Pairs in the Reaction p + $d \rightarrow p + p + n$," *Nucl. Phys.* **A157**, 209 (1970).

15. J. Sanada, S. Seki, Y. Aoki, M. Sawada, Y Tagisi, and L. S. Chuang, "Vector Analyzing Power in Final-State Interaction Region for Deuteron Break-up Reactions," in *Few Body Systems and Nuclear Forces, I*, H. Zingl M. Haftel and H. Zankel, Eds., Lecture Notes in Physics **82**(Springer-Verlag, 1978), p. 261.

16. J. Bruinsma and R. van Wageningen, "Nucleon-Deuteron Breakup Quantities Calculated with Separable Interactions Including Tensor Forces and p-Wave Interactions," Phys. Lett. **63B**, 19 (1976) and Nucl. Phys. **A282**, 1 (1977).

17. C. Stolk and J. A. Tjon, "n - d Breakup Calculations with the Reid Interaction," Phys. Rev. Lett. **39**, 395 (1977).